Characterization of optically driven fluid stress fields with optical tweezers

Gregor Knöner, Simon Parkin, Norman R. Heckenberg, and Halina Rubinsztein-Dunlop

Centre for Biophotonics and Laser Science, School of Physical Sciences, The University of Queensland, St. Lucia QLD 4072, Australia

We present a controlled stress microviscometer with applications to complex fluids. It generates and measures microscopic fluid velocity fields, based on dual beam optical tweezers. This allows an investigation of bulk viscous properties and local inhomogeneities at the probe particle surface. The accuracy of the method is demonstrated in water. In a complex fluid model (hyaluronic acid), we observe a strong deviation of the flow field from classical behavior. Knowledge of the deviation together with an optical torque measurement is used to determine the bulk viscosity. Furthermore, we model the observed deviation and derive microscopic parameters.

I. INTRODUCTION

The viscoelastic properties of liquids in biological systems, e.g., blood, largely contribute to their biological functionality. Applied shear stress can trigger functional processes in cells such as signaling or adhesion [1]. The ability to characterize these viscoelastic properties and to controllably apply stress on a microscopic scale is of great interest as it can be used for diagnostics in medicine and will lead to a better understanding of the functionality of biological systems.

Microrheology, the measurement of the viscous and elastic modulus in microscopic volumes of fluid, has received a lot of attention during the past decade. Most techniques are passive and based on monitoring the Brownian motion of probe particles in the complex fluid. Dynamic light scattering [2], laser deflection [3,4], and video particle tracking [5] have been used to measure the mean square displacement $\langle \Delta r^2(t) \rangle$, of probe particles and to calculate the complex shear modulus $G^*(\omega)$ [6]. Complex fluids can exhibit local inhomogeneities of the size of the polymer correlation length (of order of 10^{-7} m), e.g., depletion layers, causing single particle experiments to no longer reflect the bulk viscoelastic properties. By measuring the correlated motion of a pair of tracer particles, the viscoelastic properties of the fluid can be derived without knowledge of the coupling between the tracers and the medium [7,8].

Measurements of the Brownian motion of one [9] and the correlated motion of two particles [10] have also been performed in optical tweezers giving enhanced bandwidth. Although these techniques are very effective in accessing $G^*(\omega)$, they are passive in the sense that they cannot apply controlled stress to the polymer networks of complex fluids or induce stress controlled functional processes in cellular structures.

This limitation was overcome by using laser tweezers to actively rotate microscopic particles. Rotation has been achieved by a transfer of angular momentum to birefringent crystals [11,12], to asymmetric shapes like rods and chromosomes [13], and by simultaneously transferring spin and orbital angular momentum [14]. The use of spherical birefringent crystals (vaterite) allows fast controlled rotation and a

simultaneous measurement of the stress strain relationship [15]. Strain rates of 2500 s^{-1} can be produced in the equatorial plane on the surface of a vaterite rotating at 200 Hz. Measurement of the optical torque and the rotation frequency yields the fluid viscosity. Although this works very well for Newtonian fluids, the technique will be affected by the local inhomogeneities in complex fluids and the coupling between rotating particle and fluid.

In this paper, we present first quantitative measurements of the fluid velocity fields generated by optically driven microscopic particles. In the same way the extension from one particle to two particle passive microrheology proved that single particle measurements do not provide the bulk viscoelastic moduli of complex fluids [7], we show that the measurement of the fluid velocity field is essential to apply the above described technique [15] to complex fluids. The flow field measurement allows the characterization of the coupling between rotating particle and fluid. In combination with torque measurements, our system performs as a controlled stress microviscometer which can be used in complex fluids. We can create and probe microscopic flows at high shear rates without the need for large support systems (e.g., pumps), microchannels or high concentrations of tracer particles. We employ dual beam optical tweezers as a microscopic flow sensor to carry out microvelocimetry. We show the validity of the method by measuring velocity profiles in water using two experimental techniques. We show that at shear rates of 300 s^{-1}, water exhibits the expected Newtonian behavior without any slip on the particle surface. In contrast, measurements on aqueous solutions of hyaluronic acid (HA) show a strong deviation from classical behavior, most likely due to the formation of a depletion layer. Subsequent optical torque measurements allow the determination of the bulk viscosity and the estimation of the depletion layer width.

II. MICRORHEOLOGICAL TECHNIQUE

A. Flow field generation

The flow field is created by using optical tweezers to levitate and rotate a micron sized particle. We use spherical vaterite crystals, which are produced by precipitation in a pro-

cedure described in Ref. [15]. The birefringence of vaterite allows the transfer of spin angular momentum from a circularly polarized laser beam to the particle which causes it to rotate. The rotation speed can be controlled by changing either the ellipticity of the beam polarization or the incident laser power. The torque exerted on the particle by the focussed laser beam is opposed by the drag torque of the surrounding fluid which depends on the fluid viscosity. Rotation rates of 400 Hz are achieved with 2 μm vaterite crystals and few hundred mW of laser power.

B. Theory

A signal advantage of this method is that for a free rotating sphere, classical hydrodynamic theory yields analytic solutions. Starting with the Navier-Stokes equation, simplifications can be made assuming steady incompressible flow, a zero body force and low Reynolds number ($<10^{-3}$ in our system). The flow velocity **v** is then described by the homogenous Stokes equation

$$\eta \nabla^2 \mathbf{v} = \nabla p, \tag{1}$$

where p is the pressure and η the dynamic viscosity. A homogeneous particular solution of this problem in spherical coordinates is Lamb's general solution [16]. Matching of the boundary conditions and assuming no slip at the particle surface leads to the solution

$$\mathbf{v} = \omega \mathbf{e}_z \times \mathbf{x} \frac{a^3}{|\mathbf{x}|^3} \tag{2}$$

for a sphere of radius a rotating at angular frequency ω. The direction of flow is always perpendicular to the plane containing the z axis (unit vector $\mathbf{e}_z$) and the coordinate vector **x**. The fluid velocity in the equatorial plane is proportional to the reciprocal square of the distance from the sphere center. The drag torque is given by $\tau_z = -8\pi\eta a^3 \omega$ and does, in contrast to the velocity field in a homogeneous fluid, depend on the fluid viscosity. We measure this velocity profile by optical means and use it to identify any non-Newtonian behavior.

In inhomogeneous systems such as a high molecular weight polymer solution, hard wall interactions between colloidal particles and polymer molecules cause a drop in polymer concentration close to the particle surface [17,18]. As a consequence, the local viscosity near the surface is reduced. The width of this depletion layer is usually in the range of the polymer/macromolecular correlation length ξ [8].

In order to understand how this layer of reduced viscosity influences the rotation of a spherical particle when constant torque is applied, we use a simple shell model. In this model, the viscosity drops from its bulk value η_{bulk} to the local value η_{loc} at a boundary layer which is located at a distance d from the particle surface. The velocity profile outside this boundary layer is described by Eq. (2). If the particle is rotating at angular velocity ω_1 and the boundary layer at ω_2, then the velocity profile in between is given by
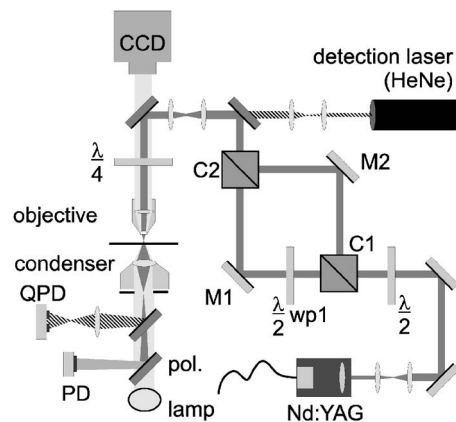

FIG. 1. The dual optical tweezers are based on a fibre coupled Nd:YAG laser. Its output is expanded and split into two beams (C1), each individually steerable with a gimbal mounted mirror (M1 and M2). A half wave plate in one arm and recombination by a 70/30 non polarizing beamsplitter (C2) allows independent polarization control. A detection laser (HeNe) and quadrant photodetector (QPD) are used to monitor probe particle deflection. The vaterite rotation frequency is measured by a linear polarizer (pol.) and photodetector (PD).

$$\mathbf{v}_{\text{in}}(\mathbf{r}) = \frac{R_1^3 R_2^3}{R_2^3 - R_1^3} \times \left[\left(\frac{1}{|\mathbf{r}|^3} - \frac{1}{R_2^3} \right) \omega_1 \times \mathbf{r} \right.$$
$$\left. - \left(\frac{1}{|\mathbf{r}|^3} - \frac{1}{R_1^3} \right) \omega_2 \times \mathbf{r} \right], \tag{3}$$

where R_1 is the particle radius and R_2 the boundary layer radius [19]. From the velocity profile, we can calculate the viscous stress tensor $\sigma'_{ik} = \eta_{\text{loc}}(\delta v / \delta r - v/r)$ at the sphere surface ($r = R_1$), which corresponds to the frictional force per unit area. The total torque τ_{drag} due to friction acting on the rotating particle can be found by integration of σ'_{ik} in spherical coordinates

$$\tau_{\text{drag}} = 8\pi\eta_{\text{loc}}(\omega_2 - \omega_1) \frac{R_1^3 R_2^3}{R_2^3 - R_1^3}. \tag{4}$$

This drag torque equals the applied optical torque τ_o in the case of a optically driven rotating particle and can be directly measured [15]. The above equation allows an estimation of the depletion layer width $d = R_2 - R_1$ as will be shown later.

C. Measurement of flow field

We probe the flow by two methods, both employing 1 μm polystyrene probe particles (Polysciences, Inc.) and fully steerable dual beam optical tweezers (Fig. 1). Trap one holds and rotates the vaterite particle whereas trap two holds the probe particle. The rotation frequency of the vaterite particle is measured in all experiments by detecting the linear polarized component of the forward scattered trapping beam which is modulated at twice the rotation frequency.

Method 1 measures the fluid velocity by monitoring the probe particle displacement in the trap due to viscous drag.

Motion of the probe particle deflects the beam of a separate detection laser (HeNe) which is registered with a quadrant photodetector (QPD). The signal is directly calibrated against movement with known velocity of the piezo actuated microscope stage. This method is especially useful as it does not require knowledge of the fluid viscosity and trap stiffness and can therefore be used with unknown liquids. The calibration curve of the detector signal to the fluid velocity does depend on the coupling between the probe particle and the fluid. Calibration is carried out directly before each experiment in the fluid that is to be probed, so the coupling is identical in an actual experiment. Therefore, the calibration takes the coupling already into account, and our measurements are not affected by any inhomogeneous effects close to the surface of the probe particle.

The sensitivity of the system can be increased by decreasing the trap stiffness and measurement of fluid speeds below 50 μm/s (corresponding to 450 fN for 1 μm probe in water) is possible. For enhanced precision and elimination of signal drift, the difference in probe displacement between rotating vaterite (flow) and stationary vaterite (no flow) is measured. The probe particle deflection is sampled at 2 kHz for 5 s at distances in the range of 1 to 18 μm.

Method 2 uses the dual trap to bring a probe particle to the desired distance from the rotating vaterite. The probe trap is switched off and due to the low Reynolds number, the probe particle instantly moves with the fluid flow. The probe particle can encircle the vaterite on a more or less stable orbit (depending on distance) for up to 6 times without a noticeable change in its vertical (z) position. Radial diffusion can cause a probe particle to explore the flow at various distances from the vaterite. The motion of the probe in the flow field is tracked by video microscopy and the flow velocities evaluated (Fig. 2).

III. RESULTS AND DISCUSSION

A. Flow field in water

The validity of both methods was established by making measurements in pure water. Figure 2(b) shows data collected for a vaterite particle with a radius of 2.6 μm rotating at 25.2 Hz using method 1. To correct for slight changes in rotation frequency [Fig. 2(a)] due to the manual adjustment of the polarization of the vaterite trapping beam, frequency normalized velocities are plotted. The least squares fit of Eq. (2) to the data agrees very well with the theoretical curve expected from particle rotation rate and size specified above.

Using video microscopy and particle tracking (method 2), the velocity profile in Fig. 2(c) was obtained for a vaterite particle with a radius of 1.8 μm rotating at 13.4 Hz. The agreement between curve fit and theoretical curve is again very good. Measurements using both methods were carried out a number of times using different sized particles and always yielded very good agreement.

Influence of the probe particle and boundaries. Both methods for measuring the fluid velocity field employ a probe particle which disturbs the flow field. In method 1, the probe is stationary and expected to cause larger disturbance compared to method 2, where the probe moves freely with
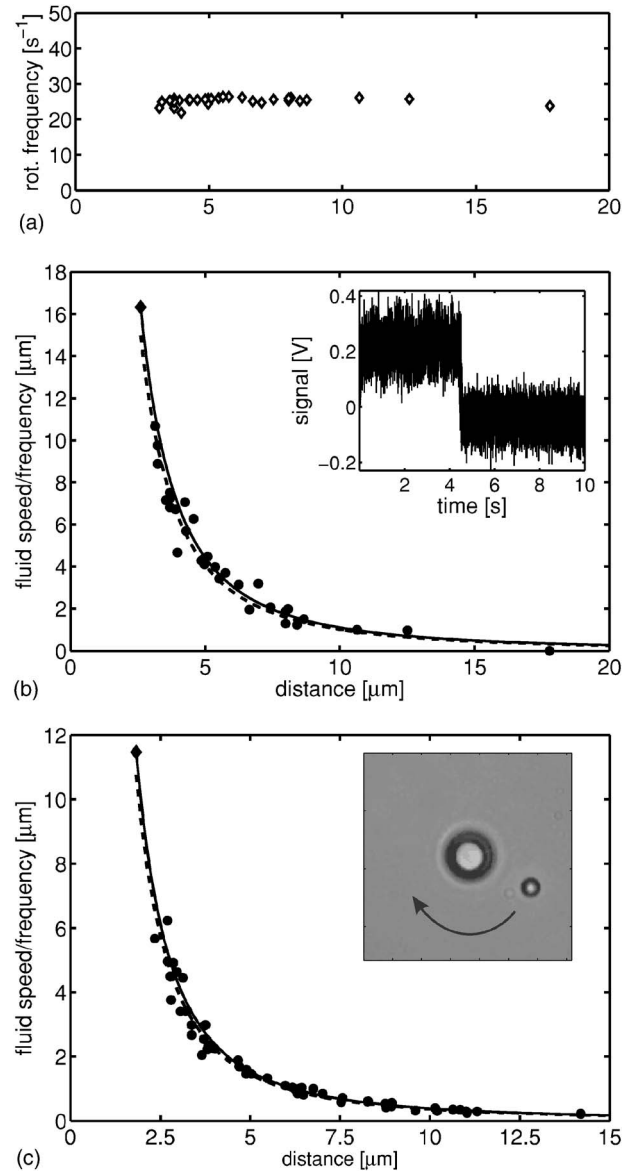

FIG. 2. (a) The vaterite rotation frequency does not depend on its distance to the probe particle. Fluctuations are due to the manual adjustment of the wave plate to obtain circular polarized light. (b) Velocity profile of a r=2.6 μm vaterite rotating at 25.2 Hz [see (a)] measured with method 1 (circles). Model (solid curve) and fit of the data (dotted) agree very well. The inset shows the position signal of the probe particle with rotation turned on/off. (c) Velocity profile of a r=1.8 μm vaterite rotating at 13.4 Hz measured with method 2 (video tracking). Again, very good agreement between model and curve fit are obtained. The inset shows a frame from a video tracking experiment (contrast enhanced for demonstration).

the flow. Quantification of the flow disturbance was the main reason for using these two methods with different degree of flow disturbance.

In method 2, the probe moves freely with the flow. Disturbance arises from the existing fluid velocity gradient, causing streamlines on the side of the probe facing the rotating vaterite to move faster than the streamlines on the opposite side. This shear will cause the probe particle to rotate thereby minimizing the disturbance. For a linear gradient, the

probe will move with the velocity of the streamline through its center. This approximation is certainly valid for probe positions further away from the rotating vaterite. Closer to the vaterite, the nonlinear gradient will cause the probe to move at the speed of a streamline off its center. Nevertheless, this deviation is negligible compared to the error in the determination of the probe particle position of ± 0.11 μm. To show the validity of these assumptions, we have fitted our model to the datapoints in Fig. 2(c) with a distance $d < 5$ μm and $d > 7$ μm. The fit for the distant datapoints deviates by -1.0% from the expected curve whereas the fit for the close points deviates by -6.0%. Both fits are within the combined error of 3% of the expected curve and of 3% of the datapoints. The deviation at closer distances may result from higher scattering of the data and the reduced statistics of both fits. A noticeable increase in the drag experienced by the rotating vaterite is not expected in this method and has not been observed, as the flow is not restricted.

This is different in method 1, where the probe is held stationary and presents a resistance to the fluid flow. The rotating vaterite experiences this resistance as an increased viscosity. Since we are applying constant torque, this results in a decrease in rotation frequency. By looking at the rotation frequencies in Fig. 2(a), we find a decrease of only 5.1% for the closest particles. From these measurements, we estimate a maximum increase in viscosity of 5.4% experienced by the rotating vaterite due to the resistance of the probe at the closest position. A theoretical estimation of this effect is a nontrivial problem and exceeds the scope of the paper. Since the increase in resistance becomes negligible at large distances of the probe to the vaterite, we again looked at curve fits to datapoints with a vaterite-probe distance $d < 5$ μm and $d > 7$ μm. We find deviations from the model of -8.6 and -1.0 %, respectively. The slightly larger deviation of close points may result from the effectively increased viscosity.

Comparing both methods, we note that although disturbance of the fluid flow is much higher in method 1, the effect on our measurements is smaller than 9% for measurements taken very close to the crystal and negligible at greater distances. Both methods yield good results for the measurement of velocity fields, and very good results if measurements are taken at larger distances (e.g., >6 μm). It is therefore concluded that both techniques are valid for determining velocity profiles on a microscopic scale.

Changing the polarization in trap 1, which is used to turn vaterite rotation on and off, does not influence the probe particle position. This was confirmed for various distances without a vaterite in the trap. Furthermore, we found that the coupling between the rotating vaterite and the medium (water) does fulfil the no slip boundary condition. The maximum observed shear rate of 300 s^{-1} did not induce slip.

Further flow disturbance may result from wall effects. We have quantified wall effects for rotating crystals by applying constant torque and measuring the change of rotation rate with wall-surface distance. Vertical walls show an effect at a distance of 1 particle diameter, whereas horizontal walls (e.g., coverslip or slide) show an effect only when the crystal is almost touching the wall. This is due to the fluid velocities, which are very small above and below the poles of the particle, and higher near the equator. Theoretical calculations
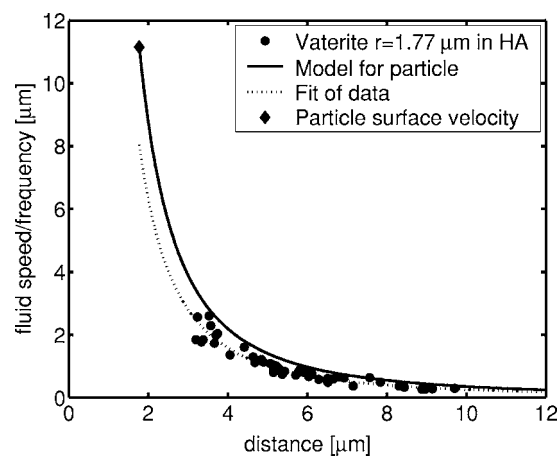

FIG. 3. The fluid velocity profile of a vaterite particle does deviate by more than 24% from the expected profile, which is calculated from the particle size $r = 1.77$ μm and the rotation frequency $f = 3.3$ Hz. The y axis is normalized by the frequency. This deviation was observed in a number of experiments.

show that the drag correction factor for a vertical wall drops to 1.01 at a distance of 1.1 particle diameters [20], and it will be much smaller for a horizontal wall. We conduct our experiments deep inside the sample, at least 6 particle diameters (i.e., 30 μm) away from horizontal walls (microscope slide and cover glass), and millimeters away from any vertical walls, hereby making any wall effects negligible.

B. Flow field in HA solution

An interesting application of flow field measurements is to test if the use of a vaterite particle as a viscosity probe is affected by a non-Newtonian environment. We measured velocity profiles in hyaluronic acid (HA). HA is a linear anionic polysaccharide. The viscoelastic properties of solutions in water strongly depend on the molecular HA concentration [21]. For our measurements, we added vaterite and probe particles to a solution of 1.5 g/l HA (rooster comb, 1.5 $\times 10^6$ Da average molecular weight) in phosphate buffered saline (PBS).

The velocity profiles obtained from this solution show clearly a deviation from the behavior of Newtonian fluids. Vaterite particles in the size range of 3−4 μm were rotating at 3−5 Hz, considerably slower than in water (approx. 30 Hz). The generated fluid flow around the particle was on average 24% lower than expected from the model parameters (Fig. 3). This deviation is significant and much larger than the error in the expected profile (3%). A fit to the points which are more than 7 μm away from the rotating vaterite shows a similar deviation of 25%. At those larger distances, the probe does not disturb the flow, which shows that the deviation is indeed a physical effect and not caused by any hydrodynamic interaction between probe and rotating vaterite.

To interpret these results, we have to consider various effects which could create such a deviation of the measured velocity profiles in a polymer solution. The effects we have to consider are the interaction of the rotating particle with the
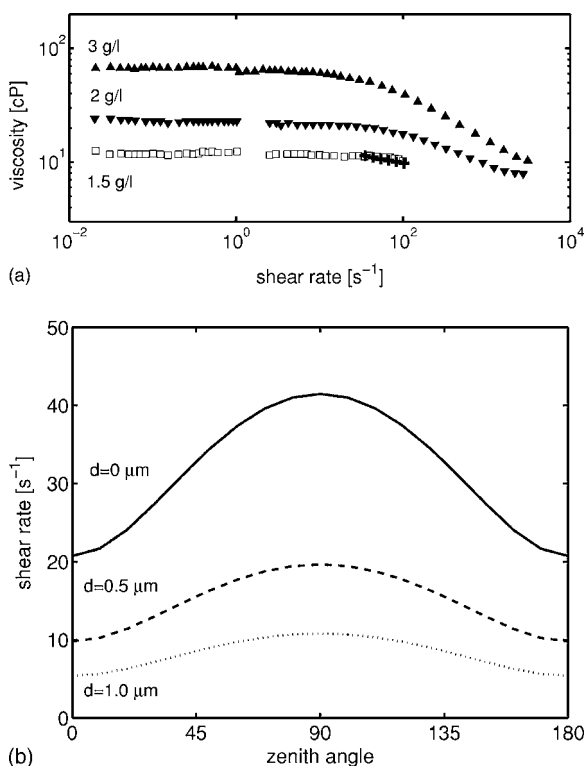
FIG. 4. Upper: Viscosity of HA of different concentrations as a function of applied shear rate, as measured with a concentric cylinder low shear viscometer and a cone and plate rheometer by Krause *et al.* [21] (▲, ▼, □). The viscosity of the sample used in this paper (1.5 g/l) was characterized for a limited number of shear rates (+) using a cone and plate rheometer and it agrees well with the values obtained by Krause *et al.* At a concentration of 1.5 g/l, slight shear thinning does only start at shear rates above 100 s^{-1}. Lower: Shear rates prevalent in a fluid when rotating a sphere of 1.77 μm radius at 3.3 Hz, as a function of distance to the sphere surface and zenith angle θ (measured from the axis of rotation). Highest shear rates occur on the surface of the sphere ($d=0$) in the equatorial plane ($\theta=90°$) and drop sharply with increased distance. The highest shear rates are below the shear rates at which shear thinning starts to occur in the concentric cylinder measurements.

solvent, the interaction with the polymer molecules, and a change in the local rheology of the solution. The coupling between the particle and the solvent, i.e., water, has been investigated in the previous section and did not show any slip. Shear induced slip can therefore not be responsible for the observed effect. In contrast to passive microrheological techniques, we induce stress, which could alter the rheological properties of the polymer solution locally by shear thinning. Shear thinning is caused by shear stress leading to molecular alignment and deformation of the polymer. The reduction in viscosity by shear thinning is highest at high shear rates and high polymer concentrations. The dilute concentration of HA employed in our experiments does not exhibit shear thinning below shear rates of 100 s^{-1} [21,22]. In our experiment, high shear rates only occur in the equatorial region on the surface of the rotating particle and are still below the limit for shear thinning (Fig. 4). This strongly suggests that shear thinning does not occur in our experi-
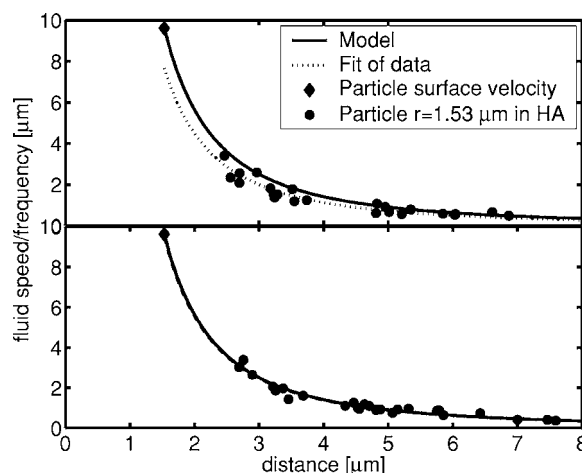

FIG. 5. Fluid velocity field around rotating vaterite particle in HA before (upper) and after (lower) attachment of a submicron sized particle. The deviation from the model observed before attachment disappears thereafter. This may be due to the destruction of a depletion layer surrounding the vaterite particle.

ments and is not responsible for the observed deviation of the velocity profile.

The polymer concentration close to the surface of colloidal particles can be decreased due to polymer-particle interaction which can be described in a hard sphere model [18,23]. In this so called depletion layer, the viscosity is decreased as it depends on polymer concentration. Depletion layers have been observed in other polymer solutions using passive microrheological techniques [8,17]. In our system, a decrease in HA concentration in proximity to the rotating vaterite particle and the resulting lower viscosity would cause the particle to rotate faster with the same applied optical torque. The resulting velocity profile would have a steep drop in the depletion layer region and would follow Eq. (2) thereafter. We believe that a depletion layer is responsible for the measured velocity profile in HA as it would create the measured deviation and is present in most systems of colloidal suspensions in polymer solutions.

To test our argument, we attached a sub micron particle (approximately 100 nm diameter) to the rotating vaterite to disturb an existing depletion layer. Measurements taken before the particle attachment show the typical 24% deviation from the expected profile, whereas measurements taken with the attached particle agree very well with the theoretical profile (Fig. 5). This leads to the interpretation that the attachment of the particle to the vaterite disturbs a depletion layer during rotation, causing the local viscosity close to the vaterite to be restored to the bulk viscosity. This increase in local viscosity is reflected in a 6.7% decrease in the mean rotation speed of the vaterite. Modeling the system as a bigger sphere with a 100 nm greater radius would lead to only half the observed change in fluid velocity. The increase in size alone can therefore not account for the effect.

C. Combination with torque measurements

The above results effectively mean that a viscosity measurement in a polymer solution based on drag torque

would underestimate the fluid viscosity by a factor F determined by the discrepancy between model and measured velocity profile. Using a particle of the same size rotating at the same frequency as in Fig. 3, we measured the optically applied torque in a similar HA solution (method in Ref. [15]). By equating optical torque and drag torque, we found a viscosity of (7.9 ± 0.5) cP. From Fig. 3, we extract a correction factor $F=0.72\pm0.02$, yielding a corrected viscosity of (11.0 ± 0.9) cP, which agrees well with $\eta=12$ cP found in the literature [21].

The above torque measurement can be used to derive microscopic parameters of the depletion layer according to Eq. (4). Rearrangement of the equation yields

$$R_2^3 = \frac{R_1^3}{1 - 8\pi(\omega_2 - \omega_1)\eta_{\text{loc}}R_1^3\tau_o^{-1}} \qquad (5)$$

for the boundary layer width R_2. Taking the particle from Fig. 3, a rotation frequency of $\omega_1 = 2\pi \times 3.3$ Hz and an optically applied torque of 2.34×10^{-17} Nm is measured. By extrapolation of the measured velocity field using the fitted curve (Fig. 3), we can estimate the rotation frequency of the boundary layer $\omega_2 = 2\pi \times 2.1$ Hz. Assuming a viscosity in the depletion layer between that of the solvent ($\eta_{\text{loc}}=1$ cP) and a third of the bulk ($\eta_{\text{loc}}=4$ cP), a depletion layer width $d=R_2 - R_1$ of 26 to 95 nm is found, respectively. It has been shown that the depletion layer width is often in the order of the polymer correlation length ξ [8,18]. In a 1.5 mg/ml solution of HA, the correlation length is $\xi=100$ nm [24] and is comparable to our depletion layer width if we use the upper value of η_{loc}. Physically, we expect the local viscosity to decrease continuously toward the particle surface. The depletion layer width is then defined at the half value of the bulk viscosity.

Although we can not yet exactly determine the depletion layer width, the above considerations clearly show that a depletion layer model can reproduce the measured velocity profiles with model parameters lying in the expected range.

IV. CONCLUSIONS

We have used two methods to precisely measure fluid velocity fields in microscopic volumes. We showed that a rotating micron sized particle in water creates a flow field that is expected from classical hydrodynamic theory. Other methods have been used to create microscopic flow fields [25,26], and our technique could be used to characterize these. In a polymer solution, we find that the flow field lies on average 24% under the profile expected from theory. We attribute that to a layer around the rotating particle in which the polymer concentration is depleted. A simple shell model is used to explain the observed velocity profile yielding a depletion layer width of the expected magnitude.

The combination of the technique with optical torque measurements allows us to measure steady state viscosities in polymer solutions at controlled shear rates. This corresponds to the passive technique of two-point microrheology. Theoretical calculations show that one-point microrheology of a semidilute polymer solution measures a viscosity of 73% of the actual bulk value [18]. We find that measuring only the optical torque gives a similar underestimation of the bulk viscosity (76% of the bulk on average), whereas the combined measurement (fluid velocity and torque) yields correct values. These experiments were carried out at low shear rates to avoid shear thinning of the polymer solution. In future experiments, we will increase the shear rate and use the measurement of the fluid velocity field to investigate the shear rate dependence of the viscosity.

[1] O. Dwir, A. Solomon, S. Mangan, G. S. Kansas, U. S. Schwarz, and R. Alon, J. Cell Biol. **163**, 649 (2003).

[2] T. G. Mason and D. A. Weitz, Phys. Rev. Lett. **74**, 1250 (1995).

[3] T. G. Mason, K. Ganesan, J. H. van Zanten, D. Wirtz, and S. C. Kuo, Phys. Rev. Lett. **79**, 3282 (1997).

[4] F. Gittes, B. Schnurr, P. D. Olmsted, F. C. MacKintosh, and C. F. Schmidt, Phys. Rev. Lett. **79**, 3286 (1997).

[5] J. C. Crocker and D. G. Grier, J. Colloid Interface Sci. **179**, 298 (1996).

[6] T. G. Mason, Rheol. Acta **39**, 371 (2000).

[7] J. C. Crocker, M. T. Valentine, E. R. Weeks, T. Gisler, P. D. Kaplan, A. G. Yodh, and D. A. Weitz, Phys. Rev. Lett. **85**, 888 (2000).

[8] D. T. Chen, E. R. Weeks, J. C. Crocker, M. F. Islam, R. Verma, J. Gruber, A. J. Levine, T. C. Lubensky, and A. G. Yodh, Phys. Rev. Lett. **90**, 108301 (2003).

[9] K. M. Addas, C. F. Schmidt, and J. X. Tang, Phys. Rev. E **70**, 021503 (2004).

[10] L. Starrs and P. Bartlett, Faraday Discuss. **123**, 323 (2003).

[11] M. E. J. Friese, T. A. Nieminen, N. R. Heckenberg, and H. Rubinsztein-Dunlop, Nature (London) **394**, 348 (1998).

[12] A. La Porta and M. D. Wang, Phys. Rev. Lett. **92**, 190801 (2004).

[13] L. Paterson, M. MacDonald, J. Arlt, W. Sibbett, P. Bryant, and K. Dholakia, Science **292**, 912 (2001).

[14] V. Garces-Chavez, D. McGloin, M. J. Padgett, W. Dultz, H. Schmitzer, and K. Dholakia, Phys. Rev. Lett. **91**, 093602 (2003).

[15] A. I. Bishop, T. A. Nieminen, N. R. Heckenberg, and H. Rubinsztein-Dunlop, Phys. Rev. Lett. **92**, 198104 (2004).

[16] S. Kim and S. J. Karrila, *Microhydrodynamics* (Butterworth-Heinemann, Stoneham, MA, 1991).

[17] R. Verma, J. C. Crocker, T. C. Lubensky, and A. G. Yodh, Phys. Rev. Lett. **81**, 4004 (1998).

[18] A. J. Levine and T. C. Lubensky, Phys. Rev. E **65**, 011501 (2001).

[19] L. Landau and E. Lifshitz, *Fluid Mechanics* (Pergamon Press, Oxford, England, 1987).

[20] M. Chaoui and F. Feuillebois, Q. J. Mech. Appl. Math. **56**, 381 (2003).

[21] W. E. Krause, E. G. Bellomo, and R. H. Colby, Biomacromolecules **2**, 65 (2001).

[22] E. Fouissac, M. Milas, and M. Rinaudo, Macromolecules **26**,

6945 (1993).

[23] E. Eisenriegler, A. Hanke, and S. Dietrich, Phys. Rev. E **54**, 1134 (1996).

[24] P. Gribbon, B. C. Heng, and T. E. Hardingham, Biophys. J. **77**,

2210 (1999).

[25] K. Ladavac and D. G. Grier, Opt. Express **12**, 1144 (2004).

[26] L. Paterson, M. P. MacDonald, J. Arlt, W. Dultz, H. Schmitzer, W. Sibbett, and K. Dholakia, J. Mod. Opt. **50**, 1591 (2003).